CrystEngComm

Accepted Manuscript

ROYAL SOCIETY OF CHEMISTRY

www.rsc.org/crystengcomm

Journal Name

RSCPublishing

ARTICLE

Periodic and incommensurately modulated phases in (2-methylimidazolium) tetraiodobismuthate(III) thermochromic organic-inorganic hybrid

Cite this: DOI: 10.1039/x0xx00000x

Received ooth January 2012,
Accepted ooth January 2012

DOI: 10.1039/x0xx00000x

www.rsc.org/

A. Gągor,[a]* M. Węcławik[b], B. Bondzior[a] and R. Jakubas[b]

(2-methylimidazolium) tetraiodobismuthate(III) (abbreviated as (2-MIm)BiI_4) hybrid undergoes structural phase transition to incommensurately modulated phase at 308 K. The relative coordinates of the modulation q-vector do not change down to 150 K indicating the stability of the incommensurate crystal packing that may be modeled by the sinusoidal wave of displacements. The transformation is triggered by the deformation of $[BiI_4^-]_n$ chains which entails ordering of 2-MIm^+ counterions that couple to the anionic substructure via weak hydrogen bond interactions. Differential scanning calorimetry (DSC) and dielectric spectroscopy methods confirm the phase transition at 308 K (I→II). Two dielectric relaxation processes that may be assigned to the dynamics of the polar 2-MIm^+ cations are present; a low frequency relaxator close to T_c and high frequency one in a wide temperature region over the phase II. The compound shows significant thermochromism characteristic for direct gap semiconductors. DOS calculations together with asymmetric local environment of bismuth ions imply the presence of the stereochemically active bismuth lone pair $6s^2$ electrons in both phases.

Introduction

The possibility of combining the rigidity and stability of inorganic frameworks and diversity of organic molecules into single structure makes organic-inorganic hybrids almost an infinite source of new materials. Among them, Pb^{2+}, Sn^{2+}, Bi^{3+}, Sb^{3+} - metal halide units arranged with various organic counter-ions appear to be highly attractive candidates for novel functional materials. To date, a great number of them have been extensively studied in order to discover new controllable nonlinear optical materials and polar media [1, 2, 3]. Metal-halide hybrids that bear Pb^{2+}, Sn^{2+}, Bi^{3+}, Sb^{3+} - halide units in combination with organic counter-ions exhibit tremendous structural diversity due to the variety of the anionic substructures that may be adopted by these metal halide salts.
An important role in creation of collective properties of these materials has to be assigned to the nonbonding valence electron pairs around metal centers. Activation of the lone pairs is crucial from the point of view of emerging phase transitions [4]. By inducing cations' of center displacements in their coordination sphere may lead to acentric phases with polar or ferroelectric properties [5, 6]. The inert lone pairs, on the other hand, are attributed to improved transport properties in semiconducting hybrids [7, 8].
The anion substructures comprise of MX_6 octahedra or MX_5 square piramids that may be linked by edges, corners or faces. The vast number of connections results in numerous polymeric (1D, 2D or 3D) or discrete (0D) units, starting with isolated octahedra and square pyramids through more complex separated clusters, poly-anionic chains and layers. Low dimensional (1D and 2D) substructures enhance physical properties associated with organic and inorganic components such as nonlinear optical response and hyperpolarizability of the cations [9, 10]. Among the family of $R_aM_bX_{(3b+a)}$, where R stands for organic cation, M for Sb(III) or Bi(III) and X for Cl, Bi, I more than 40 possible anionic forms have been known almost two decades ago [11], among only iodo-bismuthates(III) more than 60 compounds have been structurally characterized and about 20 different structural types have been revealed [12 and references therein]. The major factor that induces the formation of various metal-halide networks is templating effect of cations. The dehydration of a iodobismuthate hybrid built up from Bi_4I_{16} clusters and protonated L-cystine molecules leads to 1D BiI_4 chains and 1D helical molecular chains [13] whereas the dehydration of tris(imidazolium)$SbBr_6 \cdot H_2O$ lead to formation of pentakis(imidazolium)Sb_2Br_{11} ferroelectric with corner shared bioctahedra [14].
The polar properties in organic-inorganic hybrids based on the Sb^{+3} and Bi^{+3} ions (or metal halides MX_3) are usually associated with the organic part of the crystal structures. The long-range order of dipolar organic cations is a source of the spontaneous polarization. However, the anionic framevorks also matter. The ferroelecricity appears in all known $R_5M_2X_{11}$ crystals that possess only discrete (0D) anionic units [15].

Spontaneous polarization in certain salts, e.g. in $(CH_3NH_3)_5Bi_2X_{11}$ is comparable to this found in tri-glycine sulfate (TGS) family [16]. On the other hand in $R_3M_2X_9$ connections ferroelectricity seems to be limited to 2D anionic network, despite the fact that four various anionic substructures may be formed from MX_6^{3-} octahedra [17, 18]. Ferroelectric properties have been observed also for R_2MX_5 and RMX_4 compositions with 1D polymeric connection of polyhedra [19, 20]. The appearance of ferroelectricity in these compounds has been attributed to the deformation of inorganic chains associated with the change of the degree of stereochemical activity of the Sb^{3+} and Bi^{3+} lone pairs.

The halogenobismuthates(III) and halogenoantimonates(III) that crystallize in MRX_4 composition exhibit rich polymorphism. (4-aminopyridinium)$SbCl_4$, which appeared to have ferroelectric properties, undergoes a sequence of phase transitions form *C*2/*c* to ferroelectric phase with *Cc* symmetry at 270 K, and monoclinic $P2_1/c$ at 240 K [21]. Polymorphism has been revealed also in other pyridinium or substituted pyridinium analogs as: (PyH)$BiCl_4$ [22], (4-NH_2PyH)$SbBr_4$ [23] or (4-NH_2PyH)$BiCl_4$ [24] with phase transitions governed by the dynamics of counter-ions anchored in large voids between $[MX_4]^-$ chains. The phase transitions have an order-disorder character. They are associated with freezing of thermally induced motions of cations at low temperatures that are weakly bonded to the inorganic framework by the hydrogen bonds.

Despite the distinct number of various crystal structures in $R_aM_bX_{(3b+a)}$ hybrids and rich, temperature induced polymorphism among them this is the first report on the incommensurately modulated crystal structure in this family. Here we report the synthesis and temperature dependent single-crystal X-ray studies, dielectric properties and electronic structures on the basis of density functional theory (DFT) calculations for the new (2-MIm)BiI_4 organic-inorganic hybrid that at 308 K undergoes structural phase transition to incommensurately modulated phase. The structural relationships as well as structure-property relations are discussed. The crystals show significant thermochromism characteristic for direct gap semiconductors.

Experimental

Synthesis

The starting materials were commercial $(BiO)_2CO_3$ (Fluka, purum 80-82%) and 2-methylimidazole (Aldrich, 99%). (2-MIm)BiI4 crystals were prepared by dissolving stoichiometric amounts of $(BiO)_2CO_3$ and 2-MIm^+ in diluted HI solution. Red, needle-like single crystals were grown from an aqueous solution by slow evaporation at room temperature.

Analysis: calc. for $C_4H_7BiI_4N_2$: C, 6.01, H, 0.88; N, 3.50. Found: C, 5.96; H, 0.90; N, 3.48%. FTIR (internal vibrations of cations): 3445m, br; 3222m; 3193m; 3153m; 3137m; 3002w; 2919w; 2852w; 1610s; 1531vw; 1513vw; 1498vw; 1413vw; 1403w; 1378s; 1324w; 1289m; 1268mw; 1127mw; 1094w; 1070m; 985w; 917w; 856vw; 749w; 745s; 680m; 651m; 482w; 417w. Raman (internal vibrations of anions): 272m, br; 230m, br; 162m; 133vs; 95s; 77m.

X-ray diffraction

The x-ray diffraction data for structure solution were collected at 330, 225 and 150 K. The systematic absences observed at 330 K were compatible with the *C*2/*c* space group (monoclinic, ***b***-unique). Below 308 K on cooling additional weak reflections appeared indicating formation of incommensurately modulated phase. In modulated phase the main Bragg peaks could be attributed to the monoclinic *C*-centered cell with metrics related to the high temperature phase. The diffraction patterns were fully indexed by introducing the modulation vector $\mathbf{q}=\beta\mathbf{b}^*$; $\mathbf{H}=h\mathbf{a}^*+k\mathbf{b}^*+l\mathbf{c}^*+m\mathbf{q}$, where m denotes the order of the satellite reflections. Only the first order satellites have been observed in diffraction patterns. The Figure S1 in Supplementary Materials presents reciprocal space reconstructions of the 0kl layers at 330 and 150 K. The refined modulation vector was $\mathbf{q}=0.575(2)\mathbf{b}^*$. The centrosymmetric $C2/c(0\beta0)s0$ superspace group has been chosen basing on the systematic absences for main and satellite reflections. The symbol means that the lattice is monoclinic, **b**-unique with additional (3+1) dimensional centering (1/2 1/2 0 0) and a modulation wave vector parallel to the $\mathbf{b}^*$ axis. The two-fold rotation axis is associated with an intrinsic shift of 1/2 along the fourth dimension and the *c*-glide plane with a phase inversion of the modulation wave. The high temperature phase was solved with direct methods and refined using Shelxl program package [25] whereas the incommensurate structures were refined using JANA2006 [26]. Crystallographic data and details of the refinement are compiled in Notes section. The discussion of the superspace approach to the solution of the modulated structures can be found in several articles. The authors refer the reader to the *International Tables for Crystallography, Volume C,* and excellent review articles and references therein [27-29].

The basic structure of the incommensurately modulated phase was taken from the high temperature solution. Modulation functions were added step by step for all atoms, starting from the heaviest ones. The 2-MIm^+ counter-ion was treated as a rigid body for the translational and rotational modulation whereas the fractional coordinates as well as displacement parameters were refined for individual atoms. The distances between the carbon and nitrogen atoms have been constrained to the values form the high temperature phase. Hydrogen atoms have been introduced from geometry. The occupancy of 2-MIm^+ was modulated with a crenel function, with value 1 for x4=<0; 1/2) and 0 elsewhere. A second 2-MIm^+ position was generated in the x4 =<0.5,1> region by the two-fold rotation axis $(-x_1,x_2,-x_3+1/2,x_4+1/2)$, thus for every value of *t* either 2-MIm^+ or its equivalent exhibited full occupancy. The translational and rotational modulation of the 2-MIm^+ was described using Legendre polynomials. The occupational modulation could have been also modeled with harmonics using $0.5+o\sin(2\pi x_4)$ function. Both approaches led to very similar R-values and, having only the first order satellites, they were indistinguishable from refinements. However, the amplitude *o* of the modulation wave was not varying with temperature indicating perfect order of 2-MIm^+ in the modulated phase. Thus, the model with crenel function was used in the final refinement. First order harmonics were used to calculate positional modulation of iodide and bismuth. The refinements with second order harmonics did not improve the reliability R-factors and resulted in second order terms that were much lower than their estimated standard deviations.

In both low temperature structures anisotropic refinement of I(2) position resulted in elongated displacement ellipsoid together with nearby residual electron density along the elongated axis of ellipsoid of 4.6 e/Å^3, ca. 0.54 Å from the primary I(2) position. Splitting of the I(2) position into I(2) and I(21) lead to 1.2% and 1% decrease in R values for main and first order satellites, respectively as well as flatter difference

Fourier maps with maximum 1.08 e/Å^3. Basing on these features the split atom model for apical I(2) iodide has been introduced during the refinements at 220 and 150 K. The final refined I(2)/I(21) fractions were identical for both temperatures within the estimated standard uncertainty and equal to 0.75(1)/0.25(1). Disorder of terminal iodides that results in splitting positions is often encountered in halobismuthates(III) [30]. The sections through superspace of electron density maps confirmed continuous harmonic modulation of atoms' positions. Figure 1 presents the observed (F_o) electron density with modulation wave and difference Fourier map (F_o-F_c) for the atom I(2) which has the highest amplitude of the modulation function. As can be noted the first order harmonics describe well the I(2) modulation and the electron density residuals are low.

Table 1 Selected bond lengths and interatomic distances in (2-MIm)BiI_4 at 330 and 150 K.

Bi-I distances	Phase I	Phase II	T=150K	
Terminal		Average	Min.	Max.
Bi(1)-I(2)[1]	2.9080(6)	2.916(4)	2.879(5)	2.949(3)
Bi(1)-I(2)	2.9080(6)	2.916(4)	2.879(5)	2.949(3)
Bi(1)-I(21)[1]		2.921(11)	2.882(15)	2.988(7)
Bi(1)-I(21)		2.921(11)	2.882(15)	2.988(7)
Bridging				
Bi(1)-I(1)[2]	3.0938(5)	3.0908(9)	3.0650(9)	3.1104(9)
Bi(1)-I(1)[3]	3.0938(5)	3.0908(9)	3.0650(9)	3.1104(9)
Bi(1)-I(1)	3.2733(5)	3.2630(9)	3.2384(9)	3.2820(9)
Bi(1)-I(1)[1]	3.2733(5)	3.2630(9)	3.2384(9)	3.2820(9)
Interatomic Bi···Bi distances				
In chain				
Bi(1)···Bi(1)[4]	4.6686(2)	4.6332(6)	4.6198(6)	4.6502(6)
Bi(1)···Bi(1)[7]	7.8709(4)	7.7992(7)	7.7992(7)	7.7992(7)
Between the chains				
Bi(1)···Bi(1)[5]	9.4409(4)	9.3763(11)	9.2672(11)	9.4782(11)
Bi(1)···Bi(1)[6]	9.0934(4)	9.0163(12)	8.8042(12)	9.2348(12)

Symmetry codes (for phase I and a basic structure of phase II):(1) -x,y,-z+1/2; (2) -x,-y+1,-z; (3) x,-y+1,z+1/2; (4) 1+x, y, z (5) ½+x, ½+y, z (6) 1/5-x, ½-y, -z; (7) x, y, 1+z

Bond valence sum for the Bi atom is only slightly higher than expected and oscillates around 3.06 additionally, for all *t* values it is lower than bond valence calculated for non-modulated structure. Selected bond lengths and interatomic distances in (2-MIm)BiI_4 at 330 and 150 K are presented in Table 1 and 2.

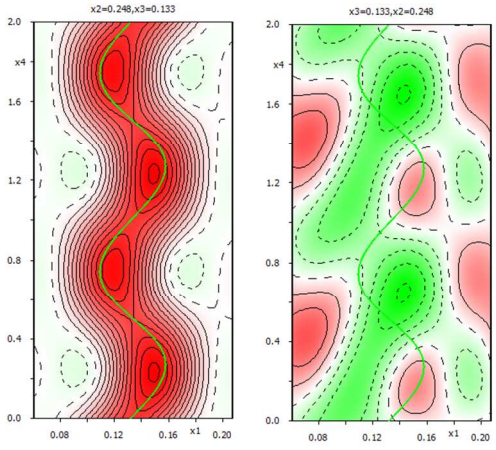

Fig. 1 The (x1, x4) section of the (3+1) dimensional superspace at the location of I(2) atom (a) observed electron density (b) difference Fourier map. The step 0.1 e/Å^3 was used for negative and positive contours.

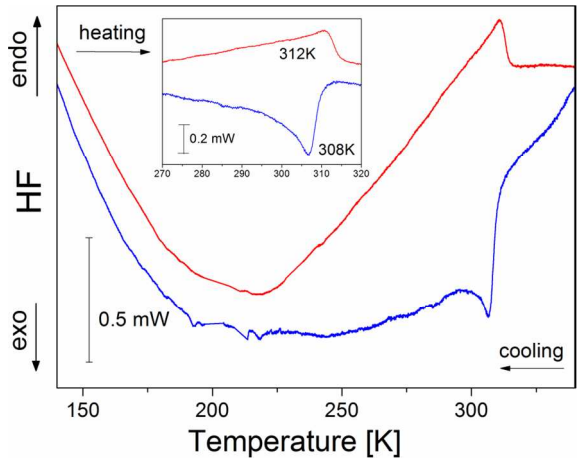

Fig 2 DSC traces for (2-MIm)BiI_4 (5K/min.).

Results and discussion

High temperature periodic phase and second order phase transition to incommensurately modulated crystal structure

Figure 2 shows DSC traces for (2-MIm)BiI_4 on cooling and heating scans. The calorimetric results clearly reveal the existence of one solid-solid reversible phase transition. The shapes of the peaks as

well as the temperature hysteresis (312 K on heating, 308 K on cooling) imply a first-order character of the transition.

The non-modulated structure (phase I) of (2-MIm)BiI_4 consists of polymeric chains of $[BiI_4^-]_n$ iodobismuthate(III) anions and stacks of 2-MIm^+ counterions. The asymmetric unit contains one Bi atom that occupies C_2 symmetry site, two iodides I(1) and I(2) on general positions and 2-MIm^+ molecule with site occupancy of 0.5. The cation is dynamically disordered over two equivalent positions that are related by the two-fold axis. Figure 3 presents the crystal packing together with the details of the crystal structure at 330 K in phase I. The polymeric $[BiI_4]^-$ anion comprises of distorted BiI_6 octahedra that form one-dimensional zig-zag chains by sharing the *cis* edges. The chains propagate along [001] direction. The stacks of counter ions are embedded in the voids between the chains. 2-MIm^+ cations are involved in weak hydrogen bond interactions with I^- ions that are too weak to overcome thermally induced in plane rotations. The donor to acceptor distances equal 3.76(1) Å for N1-H…I1 $^{-x, -y+1, -z}$ and 4.06(1) Å for N2-H…I2 $^{x, -y, z-1/2}$ bonds.

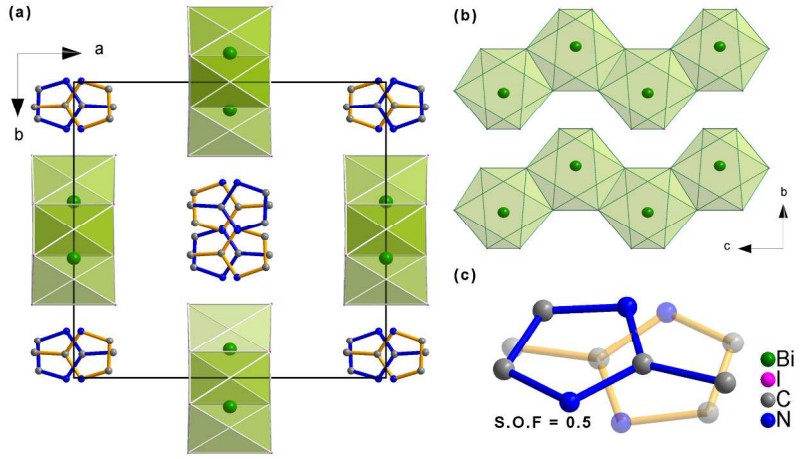

Fig. 3 (a) Packing of the (2-MIm)BiI_4 crystal structure in phase I (b), mutual arrangement of polymeric cis-$[BiI_4]_n^-$ chains (c) disorder of the 2-MIm^+ counterions, both positions are occupied with 50% probability. Hydrogen atoms have been skipped for the picture clarity.

Upon cooling the unit cell contracts in all directions. The largest decrease in distances (~1.3 % between 330 and 150 K) concerns the *c* direction. The phase transition manifests in continuous decrease of the monoclinic beta angle and step-like anomaly in *a* direction with relative decrease equal only to 0.15%. The *c* lattice parameter along which the chains propagate seems to be undisturbed. It indicates that the main structural differences between the phases should be associated with the modification of mutual distances between the chains. Figure 4 shows the temperature evolution of lattice parameters through the phase transition. Together with the subtle contraction of the unit cell additional diffraction peaks appear in the *b* direction that can be indexed by the incommensurate propagation vector **q**=0.575(2)**b***. The relative coordinates of the modulation q-vector remain almost constant in the whole measured temperature range. The incommensurate phase extends down to 100 K.

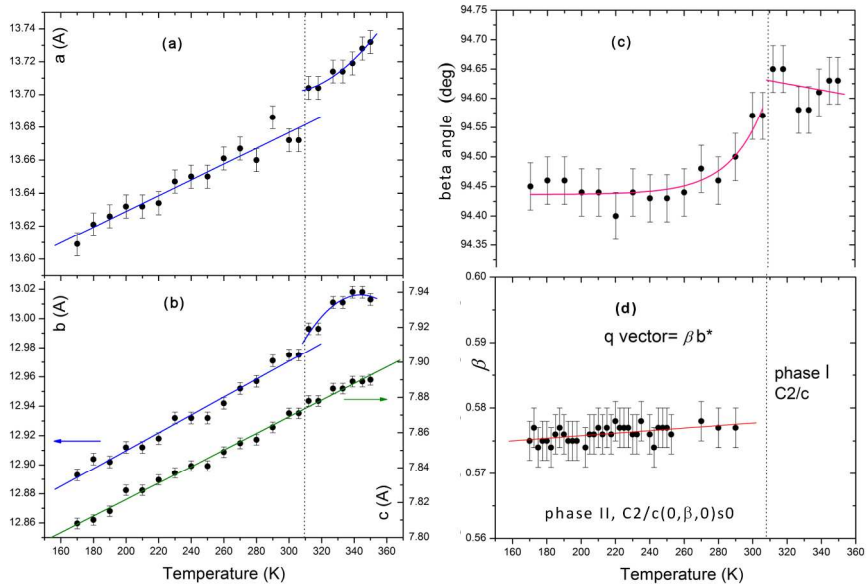

Fig. 4 Temperature evolution of lattice parameters and modulation vector **q** in (2-MIm)BiI_4. The solid lines are the guides for the eyes, the dashed line separates periodic and modulated phase (T_c=308 K on cooling).

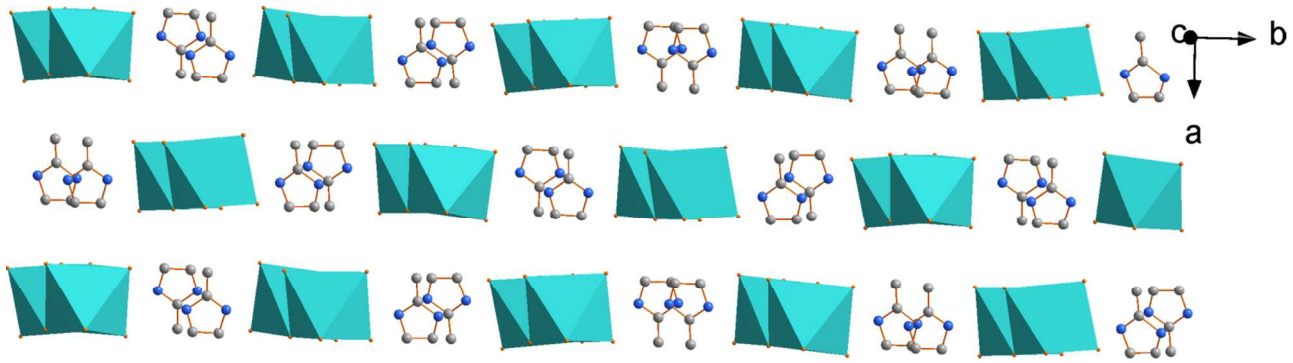

Fig. 5 The view of the five-fold approximant of the modulated structure along the c direction at T=150 K. 2-MIm$^+$ counter-ions are ordered in the modulated phase.

Incommensurate phase II

The transformation induces two main structural features. The first one concerns the 2-MIm$^+$ counter ions that order in the incommensurate phase. In each cavity the 2-MIm$^+$ adopts one of the two positions that were equivalent in the high-temperature phase. At 220 and 150 K the reorientation movements between the sites are blocked which is confirmed by dielectric response, (see the next section). Figure 5 presents five-fold approximant of the modulated structure. The (3+1) dimensional symmetry operations: the two-fold rotation axis (-x1, x2, -x3+1/2, x4+1/2) and c-glide plane (x1,-x2, x3+1/2,-x4+1/2) that induces the phase inversion of the modulation wave along the fourth dimension ($-x_1, -x_2, -x_3, -x_4$) give on average the same number of 2-MIm$^+$ cations oriented parallel and antiparallel with respect to each other in the cavities of a real crystal (physical space). Locally, however, on the length-scale of the basic cell, there are the uncompensated regions with different number of ions that are oriented in the same direction. The translations and rotations of cations are also modulated. Thus, despite the fact that the basic cell of the modulated phase is isotypic to the high temperature cell, the symmetry of the latter is broken in modulated phase.

A number of I…N contacts appears that could be related to N-H…I hydrogen bond interactions. The possible acceptors are mostly terminal iodides (I(2) and I(21), see Table 2).

Table 2 Selected I…N distances in modulated phase, T=150 K. The average, minimum and maximum values in <0,1> *t* range are tabulated.

	Average	Min.	Max.
I2-N1	3.702(12)	3.346(12)	3.882(11)
I2-N1^{ii}	3.570(11)	3.456(10)	3.784(11)
I2-N2^{iii}	3.763(12)	3.545(14)	3.853(12)
I2-N2^{iv}	3.804(13)	3.659(11)	4.133(14)
I21-N1	3.708(15)	3.293(17)	3.872(12)
I21-N1^{ii}	3.667(13)	3.568(12)	3.966(15)
I21-N2^{iii}	3.591(17)	3.246(16)	4.033(14)
I21-N2^{iv}	3.959(17)	3.610(15)	4.390(15)

Symmetry codes (for basic cell): (i) -x,-y+1,-z; (ii) -x,y,-z-1/2; (iii) -x,-y,-z; (iv) x,-y,z+1/2

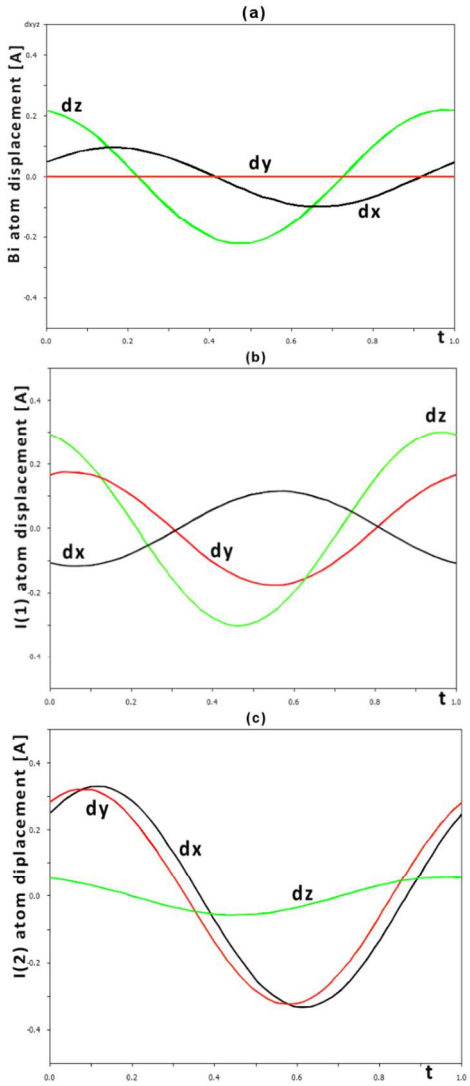

Fig. 6 Sinusoidal waves of displacements for (a) Bi (b) I(1) and (c) I(2) atoms at 150 K.

The changes in cationic substructure are only a fingerprint of much serious structural modifications that concern the anionic framework.

The second and the main feature of transformation is a collective effect which is a sinusoidal displacement of bismuth and iodide atoms from their high-temperature positions (Figure 6). The apical iodides I(2) exhibit the largest shifts perpendicular to the chains with maximal amplitude of 0.32 Å, whereas bridging I(1) atoms move distinctively in all directions with the largest shifts along the chains. I(1) atoms 'follow' bismuth displacements that reach the amplitude of 0.22 Å along the *z* direction. The first-order components of the modulation wave of Bi displacement in the *b* direction are constrained to 0 due to the symmetry restrictions. Figure 7 illustrates the evolution of mutual Bi-I distances within the single octahedron for different *t* values. The picture exposes another characteristic feature of the modulated phase. For every *t* value there are six different Bi-I distances, which implies that the bismuth coordination sphere in modulated phase has C_1 symmetry that is lower compared to C_2 in phase I. The atoms displacements affect the shape of the structural voids as well as spatial orientation of the chains that are significantly distorted that is illustrated in Figure 8.

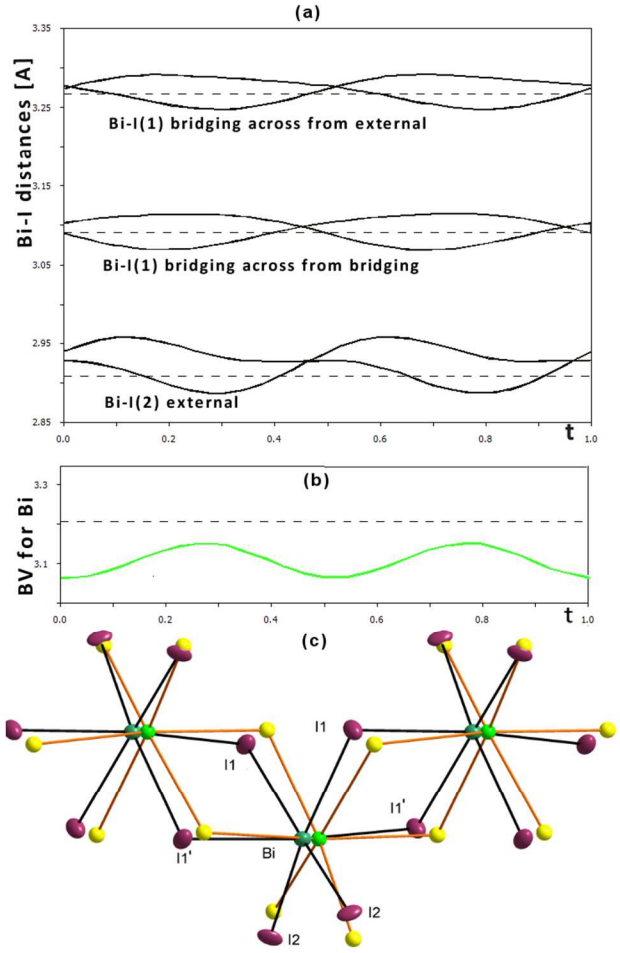

Fig. 7 (a) Bi-I distances and bond valence sum for Bi^{3+} (BV) for different *t* values in Phase II. The dashed lines stand for the non-modulated values (b) the chains of $[BiI_4]_n^-$ for t=0 (red) and t=0.6 (yellow), for t=0 the displacement ellipsoids are drawn, I(21) atom has been skipped for the picture clarity.

In $(BiI_4^-)_n$ chains there are three types of Bi-I bonds, namely: bridging across from terminal bond, terminal across from bridging bond and bridging across from bridging bond. Due to the *trans* effect [31] that occurs in halobismuthates(III) and haloantimonates(III) the shortest bonds are found for terminal bonds across from the bridging bonds and the longest are the bridging bonds across from terminal bonds. In (2-MIm)BiI_4 this trend is also observed. In the high temperature phase the difference between bridging across from terminal and terminal bonds is equal to 0.365 Å. This value is comparable to the differences in bond lengths in other iodobismuthates(III) with polymeric $[BiI_4]_n$ chains. In $[C_2H_{10}N_2]BiI_4$ H_2O [32] the difference is equal to 0.423 Å, in $[C_{10}H_9N_2]BiI_4$ 0.397 Å [33], in $[C_{18}H_{19}N_4]BiI_4$ 0.349 Å [34] and in $[C_{10}H_{10}N_1]BiI_4$ 0.339 Å [35]. It is notable that the longer the bridging bonds the shortest the terminal are. Additionally, in all compounds the real values differ from theoretically calculated distances [36, 37]. The calculations resulted in 2.987 Å for terminal across from bridging bond and 3.130 Å for bridging across the terminal bonds in $[BiI_4]^-_n$ anion, whereas in the real crystals the distances range from 2.891-2.915 Å for terminal bonds and 3.190-3.314 Å for bridging across from terminal bonds.

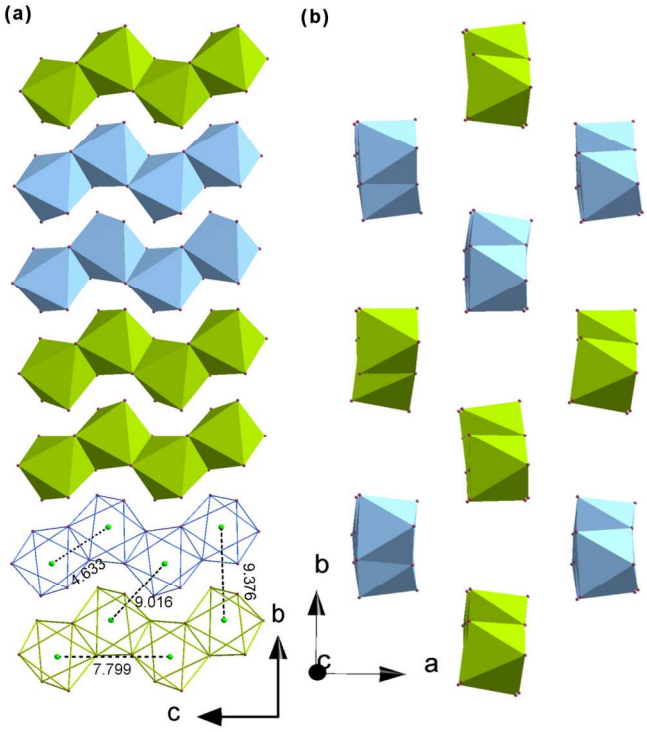

Fig. 8 (a) The view of the modulated crystal structure at T=150 K (five-fold approximant). The green and the blue chains are shifted along c direction relative to each other, the average Bi···Bi distances are drawn (b) distortion of the crystal voids which accommodate counter-ions in modulated phase.

In the modulated phase of (2-MIm)BiI_4 the Bi-I(1) bond lengths oscillate around non-modulated distances for all *t* values whereas the Bi-I(2) bonds are longer compared to non-modulated values for the most values of t. As a result, the bond valence sum of Bi at low temperature is better fitted to the expected value of 3 for Bi^{3+} compared to the parent phase. The maximum Bi-I(2) distance reaches 2.948(3) Å for Bi-I(2) (2.989(7) Å for I(21)) and approaches the theoretically calculated value of 2.987 Å for terminal across for

the bridging bonds. The elongation of the Bi-I(2)/I(21) values may be a sign of the presence of hydrogen N-H…I bonds in the modulated phase. As it is listed in Table 2 possible bonding distances may be mostly found for I(2) and I(21) terminal iodides.

Intra-chain Bi···Bi distances oscillate within the range of 4.6198(6)-4.6500(6) Å and are shorter from the corresponding distance of 4.6686(2) Å noted in the high temperature phase. Modulation preserves the "trans" effect for Bi-I bonds, although the maximum and minimum values for Bi-I(1) bridging and Bi-I(2) terminal distances do not coincide exactly. Max. Bi-I(2) and min. Bi-I(1) distances are observed for different *t* values. It should be noted however that the intra-chain bonds in modulated phase do not differ considerably from their high temperature counterparts. Much significant deviations are observed between the chains. In modulated phase their relative spatial arrangement is altered since the Bi atoms shift along the *c* axis (perpendicularly to the modulation wave) with maximum amplitude of 0.22 Å causing mutual sliding of the chains along the *c* axis. The chains may be shifted up to ~0.4 Å relative to each other inducing substantial variations within the inter-chain Bi ···Bi distances that may be crucial from the point of view of the semiconducting properties of this material. The shortest distance Bi(1)···Bi(1)^6 between the chains (see Figure 8) which is equal to 9.0934(4) in Phase I can assume values ranging from 8.8042(12) Å to 9.2348(12) Å in the modulated structure, see also Table 1.

An important role in creation of collective properties of halo-bismuthates(III) and haloantimonathes(III) play the lone pair electrons ($6s^2$ and $5s^2$) around the metal centers. The presence of the stereochemically active electron lone pair leads to an off-center displacements of the cation from the centroid of its coordination polyhedron while the change of the lone pair stereochemical activity with temperature may induce phase transitions and give rise to non-centrosymmetric crystal structures. Lone pair distortions are primarily driven by the cation-anion interactions [38] that concern mixing of cation s and anion p states mediated by the cation p states [39]. The asymmetric electron distribution exhibits strong anion dependence. Halobismuthates(III) reveal rather weak lone pair stereoactivity especially for the large iodide counter-ions thus the vast number of polar phases is encountered for the chlorides and bromides. Weak lone pair stereoactivity results in weakly distorted octahedra. The degree of distortion depends, however, also on the coordination environment and on the nature of organic counter-ions. As an example the coordination of Sn^{2+} in one dimensional SnI_3^- chains may change from regular octahedron to square pyramid when different counter ions are embedded into the crystal structure [40]. Alternatively BiI_5^{2-} units may form 0D structures with square pyramidal coordination of iodides and connected regular bi-octahedra $Bi_2I_{10}^{4-}$ [41]. In (2-MIm)BiI_4 coordination of the Bi^{3+} is significantly distorted. The terminal I(2) iodides that coordinate only to one bismuth ion are strongly bonding and attract the cation toward them, thus the bond distance is contracted compared to other atoms. This entails the bonds on the opposite side I(1) to become longer. The distance Bi-I(2) to the terminal iodide is equal to 2.9080 (1) Å at 330 K and in modulated phase may be reduced to 2.879(5) Å at T=150 K. For comparison, the shortest distance in square pyramidal coordination of Bi^{3+} that is opposite to the active lone pair is equal to 2.872 Å [41]. Taking into account the criteria defining the activity of the lone pairs through the distortions of the bismuth(III) coordination sphere reported in [42] ΔE_1=0.186(1) Å (the difference in the shortest primary and secondary distances) and ΔE_2=0.036(1) Å (the difference between the shortest distance in the coordination polyhedron of the compound under study and the known shortest distance in this element's compounds that reveal the highest lone pair stereoactivity) it may be inferred that in both phases of (2-MIm)BiI_4 bismuth lone pair is active. The change of its activity may be a trigger factor for the structural phase transition to modulated phase.

Dielectric properties

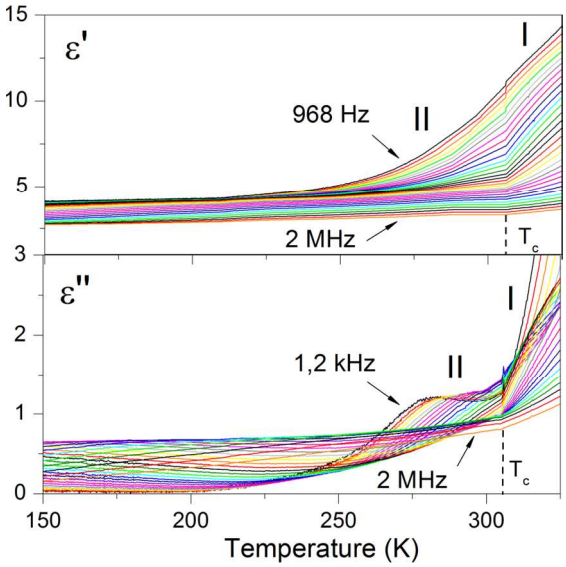

Fig. 9 The real and imaginary parts of the complex electric permittivity in (2-MIm)BiI_4.

Temperature dependence of the real and imaginary parts of the complex electric permittivity is presented in Figure 9. Over the low temperature phase (II) two dielectric relaxation processes are disclosed. The higher frequency relaxator with the dielectric increment $\Delta\varepsilon_1$ ≈1.4-1.6 is seen over a wide temperature range, whereas the lower frequency one ($\Delta\varepsilon_2$ ≈ 3.5-5) is observed in a narrow temperature range, close to T_c. The higher frequency process seems to be strongly distributed (polydispersive character). In order to characterize the dynamic dielectric properties of (2-MIm)BiI_4 the Cole-Cole formalism has been applied. The temperature dependence of the macroscopic relaxation time (τ) and Arrhenius relation are given in Supplementary Materials (see Figure S2). The activation energy E_a of the thermally activated process was estimated to be ca. 126 and 3.5 kJ/mol for the lower frequency and the higher frequency relaxator, respectively. In the high temperature phase there is observed significant increase of the electric conductivity contributing to the complex electric permittivity, thus it was impossible to estimate the dielectric parameters of the expected relaxation process. Nevertheless, taking into account the frequency

characteristic of ε" (T,ω) visible above 312 K this process may appear in the kilohertz frequency region.

Thermochromism and electronic properties of (2-MIm)BiI_4

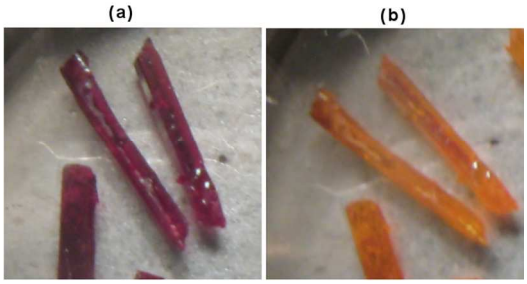

Fig. 10 (2-MIm)BiI_4 at 330 K (a) and 110 K (b).

(2-MIm)BiI_4 is a thermochromic material. It continuously changes the color with temperature from dark red at 330 K to light orange at 150 K that is illustrated in Figure 10. The color change is a clear indication of a modification of the electronic structure near the Fermi level. Thermochromic behavior in iodobismuthates(III) is primary linked with changes in interatomic Bi–I and Bi···Bi distances [43] since the absorption of the Bi^{3+} ($6s^2$) ion strongly depends on the crystal structure. It varies from ultraviolet to red [44] and depends on the coordination of Bi^{3+}, the more asymmetrical surrounding, the broader the absorption band [45]. Recently it has been shown that the degree of bonding between I···I intra-anionic pairs may influence the electronic structure as well [46]. Generally, the color changes are related mostly to the modification of anionic part because the cation electronic levels have only minor effects on the electronic structure around the Fermi level [12]. Calculated band gaps of discrete iodobismuthate polyedra and 1-D polymeric structures increase on shortening of Bi···Bi and Bi-I interatomic distances. Additionally, the energy gaps of anionic chains are lower than those of isolated ions [12, 43] thus iodobismuthates(III) experience a blue shift with reduction of dimensionality of anionic units.

Optical gap extracted from UV-vis spectroscopy at ambient temperature using the Kubelka-Munk method [47] is equal to 2 eV and is higher than band gap calculated by DFT methods (1.66 eV at 330 K). The tendency to underestimate the band gap is symptomatic in electronic band structure calculations and has been well documented in previous studies [48]. As expected from the brightening of the crystal from dark red to orange, the temperature decrease leads to an increase in the band gap. Though the change is rather slight (1.66 eV at 330K, 1.70 eV at 150K) the correct trend is preserved.

Because the cation-anion interactions are the driving force behind the lone pair distortions the DFT calculations have been performed for (2-MIm)BiI_4 for both phases to track the activity of the bismuth lone electron pair. The incommensurate structure was modeled by five-fold approximant of the modulated phase in *P*1 symmetry. Figure 11 illustrates the total density of states (DOS), exemplified by the grey area, with atomic-resolved DOS, in which the blue curve represents the states of I^- and the red curve represents the states of Bi^{3+}. It is clear that in both phases the states near the Fermi level are dominated by I^-, whereas both type of atoms make a significant contribution to the conduction band and lower part of the valence band. The main difference between the phases concerns the upper region of the valence band. In the incommensurate phase the contribution of bismuth states in total DOS increases denoting increase in mixing of I and Bi states. This picture reminds the density of states calculated for the scheelite and fergusonite form of $BiVO_4$ [49]. In the scheelite structure the bismuth lone pair is inert whereas it is active for the fergusonite structure and the main differences in the density of states between the two concern the bottom half of the valence band with only a minor changes close to the Fermi level. Increased contribution of bismuth states in total DOS in incommensurate phase may be a sign of the change in activity of the bismuth lone pair electrons after the phase transition. This interpretation is consistent with structural data that show greater deformation of the bismuth coordination geometry in the modulated structure.

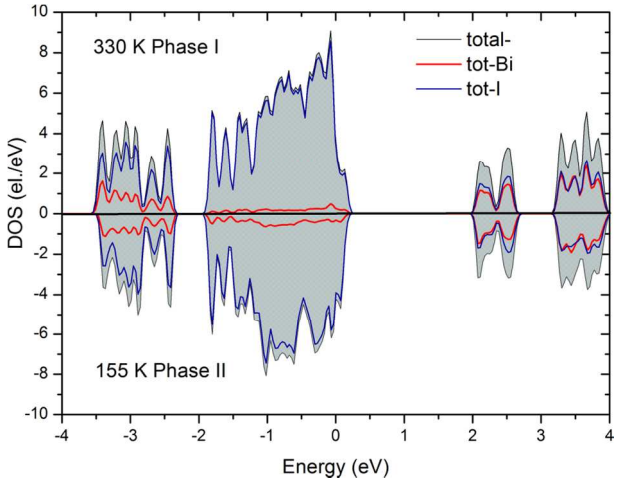

Fig. 11 Calculated total electronic density of states for $[BiI_4^-]_n$ chains in phase I and phase II (five-fold approximant of the incommensurate phase was used for calculations).

Summary

(2-MIm)BiI_4 undergoes structural first-order phase transition to incommensurately modulated phase at 308 K. The symmetry changes form *C*2/*c* to *C*2/*c*(0,*β*,0)*s*0, the modulation wave vector **q**=0.575(2)**b***. The incommensurate crystal packing is stable down to 100 K. The modulation particularly disturbs the spatial arrangement of the $[BiI_4^-]_n$ chains which leads to deformation of the crystal voids and in consequence to ordering of 2-MIm^+ counterions. The change of the lone pair activity may play the foreground role in the phase transition mechanism. The mixing of bismuth and iodide electronic states as well as asymmetrical coordination geometry of Bi^{3+} indicates that the $6s^2$ lone pair electrons are active in both phases. (2-MIm)BiI_4 shows significant thermochromism that is consistent with increase of electronic band gap with temperature lowering, calculated by DFT methods.

Acknowledgements

Part of the research (synthesis, DSC and dielectric measurements) was supported by the National Science Centre (Poland) under grant No.

2013/11/D/ST8/03297 and by the European Union under the European Social Fund.

Notes and references

[a] *W. Trzebiatowski Institute of Low Temperature and Structure Research PAS, P.O. Box 1410, 50-950 Wrocław, Poland*
[b] *Faculty of Chemistry, University of Wrocław, Joliot-Curie 14, 50-383 Wrocław, Poland*
†

X-ray data collection

Single crystals of (2-MIm)BiI_4 were selected under a polarizing microscope and mounted on a glass fiber with epoxy glue. Intensity data were collected on a KM4CCD diffractometer (κ-geometry, MoK_α radiation, λ=0:71073 Å) with the CrysAlis software under a stream of nitrogen (Oxford Cryosystem). A data set of the low temperature phase I was collected at T =330 K then the crystal was slowly cooled (2K/min) in 10 K steps and short scans with acquisition of approx. 150 reflections for temperature evolution of lattice parameters were recorded. At T=308 K additional weak reflections appeared from an incommensurately modulated phase. Without changing the crystal and orientation two sets of data collection were done at T=220 and 150 K for the structure solution. Main and satellite reflections were separated and indexed using the DataRed software. An absorption correction was applied using the multi-scan approach implemented by ADSYMM.

Crystal data and structure refinement results for (2-MIm)BiI_4 at:

330 K (phase I)
Empirical formula: C4 H7 N2 Bi I4, formula weight: 799.70, temperature : 330 K, Wavelength: 0.71073 Å, crystal system monoclinic, space group *C*2/*c*, Unit cell dimensions a=13.7359(8)Å, b=13.0043(8) Å, c=7.8727(4) (4) Å, *β*=94.636(6)°, volume 1401.66(14) $Å^3$, Z=4, Calculated density , 3.790, absorption coefficient 21.349, F(000) 1360, crystal size: 0.15 x 0.12 x 0.10 mm, θ range for data collection: 2.98 to 25.68°, limiting indices -16<=h<=16, -15<=k<=15, -9<=l<=7, reflections collected/unique: 6987/1342 [R(int)=0.0374], completeness to θ_{max} 99.6%, absorption correction: semi-empirical from equivalents, max. and min. transmission: 1.0 and 0.44, refinement method Full-matrix least-squares on F^2, Data/restraints/parameters: 1342/3/50, Goodness-of-fit on F^2: 0.937, final R indices R_1 = 0.0261, wR_2 = 0.00533, R indices (all data, [I>2σ(I)]) R_1=0.0360, wR_2 = 0.0551, Largest diff. peak and hole: 0.939 and -1.383 e/$Å^3$.

150 K (phase II)
Empirical formula: C4 H7 N2 Bi I4, formula weight: 799.70, temperature : 150 K, Wavelength: 0.71073 Å, crystal system monoclinic, space group *C*2/*c*(0β0)*s*0, **q**=0.575(2)**b***, Unit cell dimensions a=13.6187(8) Å, b=12.8788(8) Å, c=7.7992(4) Å, *β*=94.510(6)° volume 1363.69(14) $Å^3$, Z=4, Calculated density 3.894, absorption coefficient 21.943, F(000) 1360, crystal size: 0.15 x 0.12 x 0.10 mm, θ range for data collection: 2.9 to 29.78°, limiting indices -18<=h<=18, -18<=k<=16, -10<=l<=7, m=1,0,-1, reflections collected/unique: 5398/2879 [R(int)=0.054], completeness to θ=27.96 99.8%, absorption correction: semi-empirical from equivalents, max. and min. transmission: 1.0 and 0.44, refinement method: Full-matrix least-squares on F^2, Data/restraints/parameters: 2879/6/73, Goodness-of-fit on F^2: 1.17, final R indices R_1=0.0343, wR_2 =0.0822 (all), R_1=0.0286, wR_2 = 0.0743 (mean), R_1=0.0413, wR_2= 0.0897 (satellites) [I>3σ(I)], Largest diff. peak and hole: 1.12 and -1.47 e/$Å^3$.

DSC measurements

The differential scanning calorimetry (DSC) analysis of (2-MIm)BiI_4 were carried out using a Perkin Elmer model 8500 calibrated using n-heptane and indium. Hermetically sealed Al pans with the polycrystalline material were prepared in a controlled-atmosphere N_2 glove box. The measurements were made between 100 and 400 K at a rate of 5 K/min. Due to the huge background (especially on heating) a peak position of the heat anomaly was taken as the PT temperature.

Dielectric measurements

The complex dielectric permittivity, ε* = ε' –i ε'' was measured between 100 and 360 K by the Agilent 4284A Precision LCR Meter in the frequency range between 2 kHz and 2 MHz. The overall error was less than 5%. The pressed-powder pellets deposited with silver conducting glue were used. The sample before measurements was kept at 350 K and blown dry with dry nitrogen for 1h. The dielectric measurements were carried in a controlled atmosphere (N_2).
The complex electric permittivity was modeled with the Cole-Cole function:

$$\varepsilon^*(\omega) = \varepsilon_\infty + \frac{\varepsilon_o - \varepsilon_\infty}{1+(i\omega\tau)^{1-\alpha}} \quad (1)$$

where ε_0 and ε_∞ are the low and high frequency limits of the electric permittivity, respectively, ω is angular frequency, τ is the macroscopic relaxation time and the α parameter represents a measure of the distribution of the relaxation time. The activation energy E_a. was calculated according to the Arrhenius relation:

$$\tau = C\exp\left(\frac{E_a}{kT}\right) \quad (2)$$

Calculation details

Total energy calculations were performed using ab-initio density functional theory as implemented in WIEN2k ab-initio simulation package, using the FPLAPW method [46]. The calculations were performed within general gradient approximation (PBE-GGA). The plane wave basis was expanded using "charge localisation" criterion of 0.9985. The Brillouin zone was sampled with 100 wavenumbers. The self-consistent calculation was controlled by convergence of total energy of systems above 10^4 Rydberg. The spin-orbit interactions were taken into account. The calculations were simplified to the inorganic part only. The model of the crystal structure was taken from 330K and 150K. The incommensurate phase was modelled by the five-fold approximant of the modulated phase of *P*1 symmetry. The disorder of terminal iodides (I(2) and I(21)) has been simplified to more populated in the structure I(2) position.

Electronic Supplementary Information (ESI) available: crystallographic information files: 330K.cif; 150.cif, SupplementaryMaterials.docx

References

[1] A.M. Guloy, Z. Tang, P.B. Miranda and V.I. Srdanov, *Adv. Mater.,* 2001, **13**, 833

[2] N. Louvain, N. Mercier and F. Boucher, *Inorg. Chem*., 2009, **48**, 879
[3] W. Bi, N. Louvain, N. Mercier, J. Luc, I. Rau, F. Kajzar and B. Sahraoui, *Adv. Mater.*, 2008, **20**, 1013
[4] A. Gagor, M. Wojtas and R. Jakubas, *Acta Cryst. B*, 2009, **182**, 3021
[5] R. Jakubas, A. Piecha, A. Pietraszko and G. Bator, *Phys Rev B.*, 2005, **72**, 104107
[6] P. Szklarz, M. Gałązka, P. Zieliński and G. Bator, *Phys. Rev. B*, 2006, **74**, 184111
[7] Y. Takahashi, R. Obara, K. Nakagava, M. Nakano, J. Tokita and T. Inabe, *Chem. Mater.*, 2007, **19**, 6312
[8] S. Sourisseau, N. Louvain, W. Bi, N. Mercier, D. Rondeau, F. Boucher, J.Y. Buzare and C. Legein, *Chem. Mater.* 2007, **19**, 600
[9] G.A. Mousdis, G.C. Papavassiliou, A. Terzis and C.P. Raptopolou, *Z. Chem., Naturforsch. B. Anorg. Chem.,* 1998, **53**, 927
[10] D.B. Mitzi, *Prog. Inorg. Chem.,* 1999, **48**, 1
[11] L. Sobczyk, R. Jakubas and J. Zaleski, *Pol. J. Chem.,* 1997, **71**, 265
[12] W-X. Chai, Li-M. Wu, J.-Q. Li and L.Chen, *Inorganic Chemistry*, 2007, **46**, 8698
[13] W. Bi, N. Mercier, *Chemical Communications,* 2008, **44**, 5743
[14] A. Piecha, A. Gągor, A. Pietraszko and R. Jakubas, *Journal of Solid State Chem.*, 2010, **12,** 3058
[15] A. Piecha, A. Białońska and R. Jakubas, *J. Phys. Condensed Matter*, 2008, **20**, 325224
[16] R. Jakubas and L. Sobczyk, *Phase Transitions*, 1990, **20**, 163
[17] G. Bator, R. Jakubas, L. Sobczyk and J. Mróz, *Ferroelectr. Lett. Sect.*, 1987, **74**, 339
[18] J. Zaleski and A. Pietraszko, *Acta Crystallogr., Section B*, 1996, **52**, 287
[19] A. Piecha, A. Białońska and R. Jakubas, *J. Mater. Chem.,* 2012, **22**, 333
[20] W. Bi, N. Leblanc, N. Mercier, P. Auban-Senzier and C. Pasquier, *Chem. Mater.,* 2009, **21**, 4099
[21] R. Jakubas, Z. Ciunik and G. Bator, *Phys. Rev. B: Condens Matter.*, 2003, 67, 024103
[22] J. Jóźków, W. Medycki, J. Zaleski, R. Jakubas, G. Bator and Z. Ciunik, *Phys, Chem. Chem Phys.*, 2001, **3**, 3222
[23] M. Hashimoto, H. Terao, H. Fuess, I. Svoboda and H. Ehrenberg, *Bull, Chem Soc. Jap.,* 2003, **76**, 749
[24] B. Kulicka, V. Khinzybalo, R. Jakubas, Z. Ciunik, J. Baran and W. Medycki, *J. Phys. Condens. Matter,* 2006, **18**, 5087
[25] Sheldrick, G. M. *Acta Cryst.* 2008, **A64**, 112
[26] Petricek, V., Dusek, M. & Palatinus, L. (2014). Z. Kristallogr. 229(5), 345
[27] A. Schönleber, Z. Kristallogr. 2011, **226**, 499-517;
[28] T. Wagner and A. Schönleber; Acta Cryst. 2009, **B65**, 249
[29] T. Janssen, A. Janner, A. Looijenga-Vos and P.M. de Wolff, International Tables of Crystallography, Volume C, 797[30] A.M. Goforth, M.A. Tershansy, M.D. Smith, L.R. Patterson Jr., J.G. Kelly, W.J.I De Benedetti and H-C. zur Loye, *J. Am. Chem. Soc.,* 2011, **133,** 603-612
[31] J. Laane and P.W. Jagodzinsky, *Inorganic Chemistry*, 1980, **19**, 44
[32] S. Chaabouni and S. Kamoun, J. Jaud, *J.Chem.Cryst.,* 1997, **27,** 527
[33] G.A. Bowmaker, P.C. Junk, A.M. Lee, B.W. Skelton and A.H. White, *Aust.J.Chem.*, 1998, **51,** 293
[34] Y.-Y. Niu, N. Zhang, H.-W. Hou and S.W. Ng, *Acta Crystallogr. Sect. E,* 2005, **61**, 2534
[35] C. Hrizi, N. Chaari, Y. Abid, N. Chniba-Boudjada and S. Chaabouni, *Polyhedron*, 2012, **46**, 41
[36] H-L. Sheu and J. Laane *Inorganic Chemistry*, 2013, **52**, 4244-4249
[37] U. Geiser, H.H. Wang, S.M. Budz, M.J. Lowry, J.M. Wiliams, J. Ren and M. Whangbo, *Inorganic Chemistry*, 1990, **29**, 1611
[38] G.W. Watson and S.C. Parker, *J. Phys. Chem. B.,* 1999, **103**, 1258
[39] U.V. Waghmare, N.A. Spaldin, H.C. Kandpal and R. Seshadri, *Phys. Rev. B* 2003, **67**, 125111
[40] C. Lode and H. Krautscheild, *Z. Anorg. Allg. Chem.*, 2001, **627,** 841
[41] Y. Chen, Z. Yang, Ch.-X. Guo, Ch.-Y. Ni, Z.-G. Ren, H.-X. Li and J. Lang, *Eur.J.Inorg.Chem.,* 2010, 5326
[42] L.M. Volkova and D.V. Marinin, http://arxiv.org/abs/1005.3102
[43] M.A. Tershansy, A.M. Goforth, J.R. Gardinier, M.D. Smith, L. Peterson Jr. and H.-C. zur Loye, *Solid State Sciences,* 2007, **9**, 410-420
[44] A. Wolfert, E.W.J.L. Oomen, G. Blasse, *Journal of Luminescence,* 1984, **31-32**, 308
[45] C.W.M. Timmermans and G. Blasse, *Journal of Solid State Chemistry*, 1984, **52**, 222
[46] Sergey A. Adonin, M.N. Sokolov, P.A. Abramov, S.G. Kozlova, D.P. Pishchur, L.A. Sheludyakova and V.P. Fedin, *Inorganica Chimica Acta,* 2014, **419**, 19
[47] P. Kubelka and F. Munk, *Ein Beitrag zur Optik der Farbanstriche*, 1931, **12,** 593
[48] M.W. Stoltzfuz, P.M. Woodward, R. Shashardi, J-H. Klepeis and B. Bursten, Inorganic Chemistry, 2007, **46**, 3839
[49] K. Schwarz, P. Blaha, and S. B. Trickey, "Electronic structure of solids with WIEN2k," Mol. Phys., vol. 108, no. 21–23, p. 3147, Nov. 2010.

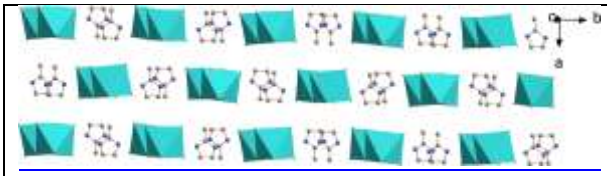

Incommensurately modulated crystal structure of (2-methylimidazolium) tetraiodobismuthate(III) thermochromic organic-inorganic hybrid.